

Seed-layer-free atomic layer deposition of highly uniform Al₂O₃ thin films onto monolayer epitaxial graphene on silicon carbide

Emanuela Schilirò, Raffaella Lo Nigro, Fabrizio Roccaforte, Ioannis Deretzis, Antonino La Magna, Angelo Armano, Simonpietro Agnello, Bela Pecz, Ivan G. Ivanov, Rositsa Yakimova, Filippo Giannazzo**

Dr. E. Schilirò, Dr. R. Lo Nigro, Dr. F. Roccaforte, Dr. I. Deretzis, Dr. A. La Magna, Prof. S. Agnello, Dr. F. Giannazzo
CNR-IMM,
Strada VIII, 5 95121, Catania, Italy
e-mail: filippo.giannazzo@imm.cnr.it
raffaella.lonigro@imm.cnr.it

Dr. A. Armano, Prof. S. Agnello
University of Palermo, Department of Physics and Chemistry,
Via Archirafi 36, 90123 Palermo, Italy

Dr. A. Armano
Department of Physics and Astronomy, University of Catania,
Via Santa Sofia 64, 95123 Catania, Italy

Dr. B. Pecz
Institute for Technical Physics and Materials Science Research, Centre for Energy Research, HAS,
1121 Konkoly-Thege 29-33, Budapest, Hungary

Prof. I. G. Ivanov, Prof. R. Yakimova
Department of Physics, Chemistry and Biology, Linköping University,
Linköping SE-58183, Sweden

Keywords: (Epitaxial graphene, SiC, Atomic Layer Deposition, Atomic Force Microscopy)

Abstract

Atomic layer deposition (ALD) is the method of choice to obtain uniform insulating films on graphene for device applications. Owing to the lack of out-of-plane bonds in the sp² lattice of graphene, nucleation of ALD layers is typically promoted by functionalization treatments or pre-deposition of a seed-layer, which, in turn, can adversely affect graphene electrical

properties. Hence, ALD of dielectrics on graphene without pre-functionalization and seed-layers would be highly desirable. In this work, uniform Al₂O₃ films were obtained by seed-layer-free thermal ALD at 250 °C on highly homogeneous monolayer (1L) epitaxial graphene (EG) (>98% 1L coverage) grown under optimized high temperature conditions on on-axis 4H-SiC(0001). The enhanced nucleation behavior on 1L graphene is not related to the SiC substrate, but it is peculiar of the EG/SiC interface. Ab-initio DFT calculations showed an enhanced adsorption energy for water molecules on highly n-type doped 1L graphene, indicating the high doping of EG induced by the underlying buffer layer as the origin of the excellent Al₂O₃ nucleation. Nanoscale current mapping by conductive atomic force microscopy showed excellent insulating properties of the Al₂O₃ thin films on 1L EG, with a breakdown field >8 MV/cm. These results will have important impact in graphene device technology.

Introduction

The deposition of uniform and high quality ultrathin insulators onto graphene represents a key requirement for the fabrication of field effect transistors,^[1,2] sensors,^[3] as well as novel ultrahigh-frequency devices^[4,5,6] based on this widely investigated two-dimensional (2D) material. Among the different physical and chemical deposition techniques available to date, atomic layer deposition (ALD) is the most promising one to achieve uniform and conformal insulators with sub-nanometer thickness control, thanks to its layer-by-layer growth mechanism.^[7] However, in the case of graphene, the lack of out-of-plane bonds or surface groups in the *sp*² lattice typically represents the principal drawback to the starting of ALD growth. Hence, the most common approaches to enable uniform ALD on graphene consist of the creation of functional groups directly on the graphene itself or the deposition of a seed-layer on the graphene surface.^[8]

Direct functionalization of graphene has been obtained by exposure to plasma or reactive gases,^[9,10] performed either ex-situ or inside the ALD chamber, or using wet-chemical treatments or

dipping the graphene in H₂O before processing.^[11] In most of the cases, plasma or reactive gas treatments convert part of the sp^2 bonds to out-of-plane sp^3 bonds, allowing the attachment of functional groups on graphene. On the other hand, the disruption of the sp^2 backbone of graphene results in the deterioration of its electrical properties, such as the electron mean free path and carrier mobility.

The seeding layer methods proposed so far include coating graphene with polymer thin films or self-assembled monolayers (SAMs),^[12] the physical deposition of thin metal films subsequently oxidized in air^[13,14] or the direct deposition of metal-oxide layers.^[15] In most of the cases, these seed layers are deposited ex-situ, i.e. outside the ALD chamber. In-situ growth of metal-oxide (Al₂O₃, HfO₂) seed-like layers by low-temperature water-assisted ALD has been also recently explored.^[16,17,18] Although the use of seed-layers does not significantly affect the sp^2 structure of graphene, the final seed-layer/insulator stack typically exhibits an increased equivalent oxide thickness with respect to a dielectric film deposited by pure thermal ALD. Furthermore, the presence of electrically active defects at the interface between graphene and the seed-layer can be responsible of charge trapping effects commonly observed in graphene devices.^[18]

From the discussion above, it is clear that ALD of dielectrics on graphene without pre-functionalization and seed-layers would be highly desirable. Previous investigations focused on thermal ALD on the pristine (i.e. untreated and seed-layer-free) graphene surface^[19,20,21,22] showed that the uniformity of the deposited films can be tailored, to some extent, by properly tuning the deposition parameters, especially the temperature and the precursors residence time.^[22] More interestingly, for similar deposition conditions, the quality of the deposited films strongly depends on the kind of graphene used, i.e. on the graphene synthesis method, the growth substrate, and eventual transfer processes from the native substrate to foreign ones.

As an example, in the case of high quality graphene flakes mechanically exfoliated from highly oriented pyrolytic graphite (HOPG), ALD growth was found to occur preferentially at the edges

of the flakes.^[19] In the case of polycrystalline graphene grown by chemical vapour deposition (CVD) on catalytic metals (Cu or Ni) and transferred to insulating substrates (such as SiO₂), material deposition during ALD typically occurs at the grain boundaries of graphene domains and at nanoscale corrugations (wrinkles) of the graphene membrane^[23] where the enhanced reactivity is ascribed to the local strain of C-C bonds.^[24,25] Furthermore, the transfer process typically leaves polymeric residues on the graphene surface, which can help in promoting the ALD nucleation. Interestingly, uniform deposition of Al₂O₃ thin films by standard ALD with H₂O and *Trimethylaluminum* (TMA) precursors has been demonstrated on monolayer CVD graphene when it was residing on the native metal substrate (Cu or Ni-Au), whereas non-uniform growth was observed for multilayer graphene on the same substrates.^[26] The enhanced nucleation in the case of monolayer graphene on the native metallic substrate was explained by the presence of polar traps at the interface with the metal, which allows an increased adsorption of water molecules onto graphene during the ALD process using H₂O as co-reactant. The strength of the electrostatic interaction with interface polar traps is obviously reduced in the case of multilayer graphene, thus resulting in an inhomogeneous Al₂O₃ coverage.^[26] These results showed how the graphene/substrate interaction and graphene thickness can play a crucial role on the ALD nucleation uniformity. At the same time, they suggest a route towards seed-layer-free ALD on pristine graphene, by taking advantage of this interaction.

Epitaxial graphene (EG) grown by thermal decomposition of SiC (0001)^[27,28,29] is another graphene-based material system especially relevant for high-end applications, such as metrology, sensing, and high frequency transistors.^[1,30,31] Contrary to the case of CVD grown graphene on metals, EG can be readily used for most of these applications, without need of transfer procedures responsible of contaminations and damages. Furthermore, EG exhibits a precise single crystalline alignment with the SiC substrate, due to the specific growth mechanism, mediated by the formation of an interfacial carbon layer (the so-called buffer layer) with partial sp³ hybridization with the Si face.^[32,33] This peculiar interface structure makes EG

compressively strained, and the electrostatic interaction with the dangling bonds at the buffer layer/SiC interface is responsible for a high n-type doping (10^{13} cm^{-3}) of the overlying graphene.

^[34] One of the main challenges in EG growth is achieving uniform monolayer (1L) graphene coverage on the entire surface. As a matter of fact, EG thickness uniformity depends on the Si sublimation conditions (temperature, pressure) and on the substrate morphology, in particular the miscut angle, with better uniformity achieved for low miscut angle SiC. EG grown under typical conditions ($T=1650^\circ\text{C}$, $P=900 \text{ mbar}$) on “nominally” on-axis SiC(0001) is commonly composed by monolayer domains on the planar (0001) SiC terraces, separated by long and narrow bilayer (2L) or tri-layer (3L) graphene stripes at SiC step edges. ^[29] Such steps are inherent of SiC due to its crystal structure, and the preferential formation of 2L and 3L graphene at their edges is related to the enhanced Si-desorption from these locations due to the weaker bonding in the SiC matrix.

ALD of thin insulators (like Al_2O_3 or HfO_2) on such pristine EG samples typically resulted in a non-uniform coverage,^[35,36] with poor or no oxide nucleation in the vicinity of the step edges, corresponding to 2L or 3L EG regions.^[35] However, the mechanisms of the different nucleation behaviour between monolayer and bilayer areas are still unclear. Furthermore, approaches to improve the nucleation uniformity in EG need to be explored.

In the present paper, highly homogeneous EG samples (with >98% 1L coverage and the remaining ~2% 2L regions confined in small patches) were grown under optimized high temperature conditions on on-axis 4H-SiC. Uniform and conformal (pinhole-free) Al_2O_3 films were obtained on these samples by thermal ALD without any seeding layer or pre-functionalization, except for the small 2L areas. Highly inhomogeneous Al_2O_3 coverage was, instead, obtained under identical ALD conditions on monolayer graphene transferred to 4H-SiC(0001), thus demonstrating that the unusual graphene reactivity is not related to the SiC substrate, but it is peculiar of the EG/SiC interface. Ab-initio DFT calculations showed an enhanced adsorption energy for water molecules on monolayer graphene with increasing n-type

doping, indicating the high doping of EG induced by the underlying buffer layer as the origin of the excellent Al₂O₃ nucleation. Nanoscale resolution current mapping by conductive atomic force microscopy (CAFM) showed excellent insulating properties of the Al₂O₃ thin films on monolayer EG.

2 Results and discussion

The EG samples used for these experiments were obtained by thermal decomposition of nominally on-axis 4H-SiC (0001) at a temperature of 2000 °C in inert gas (Ar) at atmospheric pressure using a RF heated sublimation reactor. By using specific well-controlled growth conditions (temperature distribution in the growth cell, temperature ramping up and base pressure) very uniform monolayer EG coverage on most of the SiC surface was obtained. This can be easily deduced from reflectance mapping of the samples surface, which is a straightforward method to evaluate the number of layers distribution on large area EG samples by comparing the graphene thickness dependent reflected power with that of a bare 4H-SiC substrate.^[37] A representative reflectance map of as-grown EG collected on a 30 μm ×30 μm sample area is reported in **Figure 1(a)**. Here the small yellow patches, corresponding to 2L graphene regions, cover only 1.3% surface and are surrounded by 1L graphene background on the 98.7% the area. By analysis of many reflectance images taken on several sample positions, a 1L graphene coverage >98.5% was estimated. A representative AFM morphology and the corresponding phase map on a 30 μm ×30 μm sample area are also reported in Figure 1(b) and Figure 1(c), respectively. The morphological image shows the typical stepped surface of 4H-SiC (0001) resulting from the step bunching phenomenon occurring during high temperature annealing. The variable contrast in the phase image originates from the different electrostatic force gradients experienced by the oscillating AFM tip at different surface positions; hence, it can provide information on the variation in the number of graphene layers at different positions.^[38,39] In particular, the small elongated patches with higher phase contrast in Figure 1(c)

correspond to the 2L regions in the reflectance maps in Figure 1(a). The histogram of phase values extracted from the phase map is shown in Figure 1(d), which exhibits a main peak at lower phases (associated to 1L graphene covered region) and a small shoulder at higher phases (associated to the 2L graphene patches). By integration of the counts under the two peaks, 1L coverage of 99% and 2L coverage of 1% of the surface area was deduced, which is consistent with the percentages evaluated from reflectance maps. Finally, Figure 1(e) and Figure 1(f) show a higher resolution AFM morphology and a height line profile in a region including a 2L patch. The ~ 1.3 nm and ~ 1.1 nm step heights in the line profile are associated to the SiC substrate steps, whereas the ~ 0.4 nm step is the typical step height at the boundary between the 2L region and the 1L one in the EG. [29]

These highly uniform EG samples were employed, without any pre-functionalization and seeding layer pre-deposition, as substrates for thermal ALD of Al_2O_3 thin films at a temperature of 250 °C, using TMA and H_2O as the Al source and co-reactant, respectively. **Figure 2** reports a complete structural and morphological characterization of an Al_2O_3 film obtained after 190 deposition cycles. A nominal film thickness of 15 nm was expected for this number of ALD cycles, according to the 0.08 nm/cycle deposition rate previously evaluated on reference silicon substrates. [40,41] Figure 2(a) shows a high resolution cross-sectional TEM image of the deposited Al_2O_3 film on EG/4H-SiC(0001). The monolayer EG plus the underlying buffer layer can be clearly identified at the interface between Al_2O_3 and SiC. The measured Al_2O_3 thickness is 12 nm, i.e. thinner than the nominal one, which can be ascribed to a lower growth rate of Al_2O_3 on the graphene surface probably in the early stages of the deposition process. The amorphous Al_2O_3 layer shows uniform contrast in all its thickness, indicating a uniform density of the material for this seed-layer-free ALD deposition. The appearance of nanocrystalline features at the interface with graphene and at the Al_2O_3 surface represent an artifact of the TEM measurement, i.e. the crystallization of amorphous Al_2O_3 under the electron beam irradiation. Such a phenomenon has been reported by different authors, [42] and the crystallization rate was

found to depend on the beam current. Although we tried to use a wide and spread e-beam for TEM imaging, crystallization of Al_2O_3 started to occur at the interfaces. Finally, the polycrystalline stripe on the top of the layer is a Pt shielding cover deposited before FIB (Focused Ion Beam) thinning of the TEM lamella. In order to evaluate the morphological homogeneity of the deposited Al_2O_3 , large area scans have been carried out in different sample positions. Figure 2(b) shows a representative morphological image on a $20\ \mu\text{m} \times 20\ \mu\text{m}$ scan area. The Al_2O_3 film is conformal with the topography of the EG/4H-SiC surface (see, for comparison, Figure 1(b)), except for some small depressions showing the same elongated shape of the 2L graphene patches. Figure 2(c) shows the resulting histogram of height values, where the small depression can be associated to the asymmetric tail at lower heights. The sum of the counts in this region of the distribution corresponds to $\sim 1.2\%$ of the total area, in agreement with the typical percentage of bilayer regions present in EG. A higher resolution AFM morphology of a region at the boundary with one of these small patches is reported in Figure 2(d). A very compact Al_2O_3 film with small grains can be observed on top of 1L Gr, whereas a less compact film with larger grains separated by small depressions (down to 2 nm) is found on the 2L graphene region (see the linescan in Figure 2(e)).

Besides the 12 nm thick Al_2O_3 film, obtained after 190 deposition cycles, thinner films have been also grown on EG under the same conditions, using a reduced number of cycles. In the Supporting Information a representative AFM image of Al_2O_3 obtained with 80 deposition cycles has been reported, showing a very similar morphology to that of the thicker film in Figure 2(d).

In order to evaluate the changes eventually induced by the thermal ALD process at 250°C on the structural quality and doping/strain of underlying EG, Raman spectroscopy measurements were carried out both on the virgin EG sample and after the Al_2O_3 deposition. Two representative Raman spectra for the two cases are reported in **Figure 3**, after normalization and subtraction of the SiC substrate signal (see Supporting Information). The characteristic G

and 2D peaks of graphene have been fitted with single Lorentzian functions. The values of the FWHM for the 2D peaks in these representative spectra are consistent with the 1L nature of epitaxial graphene.^[43] The small changes in the positions of the G and 2D peaks after the Al₂O₃ deposition indicate that the ALD process does not significantly affect the doping and strain of the EG. The features in the 1200 – 1500 cm⁻¹ range are related, in part, to the buffer layer at the interface between EG and the silicon face of the SiC substrate. These are overlapped to the defects-related D peak spectral region of graphene, making it difficult to evaluate eventual changes in the defectivity induced by the ALD process. However, Raman spectra measured on graphene transferred onto 4H-SiC, where buffer layer features are absent, clearly show that no defects are introduced by the ALD process, as it will be discussed later in this paper.

It is worth emphasizing that, to the best of our knowledge, such highly uniform Al₂O₃ coverage of graphene by a seeding-layer free thermal ALD at a standard deposition temperature of 250 °C has not been previously reported in the literature. Here, we ascribe the uniformity of the deposited Al₂O₃ to the excellent monolayer graphene homogeneity of these EG samples.

To support this idea, we carried out seed-layer free thermal ALD of Al₂O₃ under identical conditions on a different EG sample, obtained by high temperature decomposition of a 4H-SiC(0001) substrate with 4°-off miscut angle. Differently from on-axis SiC(0001), uniform monolayer graphene coverage cannot be typically achieved on off-axis substrates, due to the higher density of steps (nucleation sites for EG) resulting in a fast growth kinetics. In most of the cases, multilayer graphene formation is reported in the literature.^[39] Under optimized conditions, we obtained a mixed coverage with 1L and 2L graphene on most of the SiC surface. A representative reflectance map collected on as-grown EG on the 4°-off SiC substrate is reported in **Figure 4(a)**, from which nearly equal percentages of 1L (~43.4%) and 2L (~43%) graphene was deduced. In addition, ~10.3% of 0L (i.e. the carbon buffer layer) and ~3.3% of 3L coverage could be estimated. Figure 4(b) and Figure 4(c) show typical AFM morphology and phase contrast maps of this sample. As compared to EG on on-axis SiC, a significantly

higher surface roughness can be observed, due to the strong step bunching effect occurring during the high temperature treatment for graphene formation. More interestingly, the phase contrast variation in Figure 4(c) is fully consistent with the inhomogeneous graphene thickness distribution shown by the reflectance map (Figure 4(a)).

Two typical AFM morphologies (at different magnifications) of the Al_2O_3 deposited on this EG sample are reported in Figure 4(d) and Figure 4(e). In this case, regions covered by a continuous Al_2O_3 film coexist with partially or totally uncovered regions in a micrometer scale area. Figure 4(f) shows a height linescan extracted along the dashed line indicated in Figure 4(e). From Figure 4(d) and Figure 4(e), it is evident that the Al_2O_3 uncovered or partially covered regions follow the elongated pattern of SiC steps, similarly to the reflectance and phase maps in Figure 4(a) and Figure 4(c). This is a very different scenario with respect to the one observed for highly uniform monolayer EG in Figure 2. Notably, the inhomogeneous Al_2O_3 deposition obtained on such a sample with varying EG thickness resembles the typical results reported in the literature for seed-layer free ALD on EG. ^[35]

The results shown so far would lead to the conclusion that a highly homogeneous Al_2O_3 coverage can be achieved by seed-layer-free ALD on laterally uniform epitaxial graphene on 4H-SiC(0001), whereas the presence of 2L or 3L regions give rise to a locally inhomogeneous deposition. In the following, the physical/chemical mechanism responsible of such different nucleation/growth behaviour will be explored.

Firstly, we would like to clarify the role played by the 4H-SiC substrate and by the peculiar interface between graphene and SiC, i.e. the presence of the carbon buffer layer, in the EG system. To this aim, a single layer of graphene grown by CVD on copper was transferred to the surface of a virgin 4H-SiC(0001) sample. A highly homogeneous monolayer graphene coverage of SiC is obtained by an optimized transfer procedure. ^[44] However, the resulting transferred graphene (TG) on SiC is very different from monolayer EG on SiC, due to the lack of the C buffer layer and of any epitaxial orientation with respect to the substrate.

Figure 5(a) reports an AFM morphology of Al₂O₃ with nominal 15 nm thickness deposited onto TG on SiC using identical ALD growth conditions as those employed for the EG samples. An inhomogeneous nucleation, giving rise to 3D Al₂O₃ islands growth can be deduced from this image and from the representative linescan in Figure 5(b). The histogram of the height values extracted from Figure 5(a) is reported in Figure 5(c). This distribution exhibits two very distinct peaks, corresponding to the uncovered and Al₂O₃-covered graphene areas. The scenario illustrated by Figure 5(a) is the typical one observed in the case of seed-layer free ALD growth onto monolayer graphene transferred to other substrates, like SiO₂.^[26]

Figure 6 shows the comparison of two representative Raman spectra of monolayer EG and of TG onto 4H-SiC(0001), after ALD of Al₂O₃. Both spectra have been, first, normalized to the intensity of the SiC substrate signal and, therefore, subtracted for the spectral features of SiC (see Supporting Information). The EG Raman spectra exhibit a blue-shift of the G and 2D peaks positions and much lower I_{2D}/I_G intensity ratio with respect to the case of transferred graphene. The FWHM of these two characteristic peaks, obtained by single Lorentzian fit, are also reported in Figure 6. The low I_{2D}/I_G ratio for EG can be ascribed to the high n-type doping of EG induced by the interfacial buffer layer.^[34,45] Furthermore, the very large blue shift of the 2D peak in the case of EG is due to the compressive strain of this material, due to the stronger coupling with the substrate via the buffer layer.^[32] A correlation analysis of the 2D and G peaks positions^[46] (see Supporting Information) allowed to estimate an n-type doping of 1.1×10^{13} cm⁻² and a compressive strain $\varepsilon = -0.37\%$ of EG on SiC with thermal Al₂O₃ on top. A smaller compressive strain $\varepsilon = -0.07\%$ and a p-type doping $\sim 5 \times 10^{12}$ cm⁻² was evaluated for the TG with non-uniform Al₂O₃ coating. The spectral features between ~ 1250 and ~ 1600 cm⁻¹ in the EG spectrum, associated with the underlying buffer layer,^[47] are obviously absent in the Raman spectrum of TG. It is worth noting that the absence of a D peak at ~ 1300 cm⁻¹ in the spectrum

of TG, with deposited Al_2O_3 on top, confirms that no damage is produced in graphene by the thermal ALD at 250°C .

The morphological and Raman data in Figure 5 and Figure 6 demonstrate that the uniform and conformal Al_2O_3 deposition achieved on monolayer EG is not related to the SiC substrate itself, but to the peculiar properties of the interface between the EG and SiC, i.e. the presence of the buffer layer, which is responsible of a high n-type doping and strain of EG. Several recent literature works reported on the enhanced reactivity of graphene to chemical species, like diazonium molecules or metal ions, when subjecting the graphene membrane to significant mechanical strain (up to 15 %) ^[48] or doping (e.g. by field effect using a back-gate).^[49] Furthermore, it has been recently demonstrated how the contact angle of water droplets on the graphene surface can be changed by field-effect modulation of the doping. ^[50] These studies have been mainly carried out with CVD grown graphene transferred onto flexible substrates for studies on the effects of strain,^[48] and on a SiO_2/Si backgate for studies on the effects of doping.^[49] Recently, Giusca et al. reported on the impact of graphene layer thickness for water affinity to EG, with an enhanced water adsorption on 1L regions as compared to 2L ones, that was justified in terms of the different electronic structure between 1L and 2L of graphene. ^[51]

Based on these recent literature reports, our experimental findings on the optimal ALD growth of Al_2O_3 onto uniform monolayer EG samples can be mainly explained in terms of the enhanced physisorption of the water precursor, originating from the high electrostatic doping of EG induced by the buffer layer/SiC dangling bonds. This explanation is also consistent with the poorer Al_2O_3 nucleation on the 2L EG patches, since it is known that 2L EG experiences a reduced doping from the buffer layer. ^[43]

To get further insight on the doping-related enhancement of water affinity to monolayer graphene, we performed ab-initio DFT calculation of the adsorption energy of water molecules on an ideal free-standing graphene layer, by changing the Fermi level position with respect to the Dirac point $E_{\text{F}}-E_{\text{D}}$, from 0 (neutral graphene) to 0.45 eV, corresponding to a graphene n-

type doping close to the value for monolayer EG on SiC, i.e., $n=q^2(E_F-E_D)^2/\pi\hbar^2v_F^2=1.5\times 10^{13}$ cm^{-2} (q being the electron charge, \hbar the reduced Planck's constant, and $v_F=1\times 10^6$ m/s the electron Fermi velocity in monolayer graphene). As shown in **Figure 7**, the water adsorption energy increases from ~ 127 to ~ 210 meV with increasing the n-type doping in this range. We also carried out DFT calculations of the adsorption energy of the TMA molecule on a graphene surface as a function of the Fermi level of graphene. However, the increasing trend of adsorption energy with doping, previously observed in the case of the water molecule, was not verified for the adsorption of TMA on graphene. This indicates that, in the ALD process, doping is beneficial only for the wettability of the graphene surface by water. Since molecules physisorption on a surface is a thermally activated phenomenon, the time of residence of a water molecule on graphene at a temperature T depends exponentially on the adsorption energy E_a as $\tau\sim\exp(E_a/k_B T)$, k_B being the Boltzmann constant. Hence, for the typical temperature of the ALD process ($T=250$ °C), the enhanced adsorption energy of water on the highly n-type doped graphene translates into ~ 6 times increase of the residence time with respect to the case of intrinsic graphene. This longer residence time of physisorbed water molecules provides a larger number of reactive sites for Al_2O_3 formation during subsequent pulses of the Al precursor.

After assessing the morphological uniformity of the deposited Al_2O_3 films on our monolayer EG samples, the electrical quality of these insulating layers was also evaluated by conductive atomic force microscopy (C-AFM) for current mapping and local I-V analyses. ^[18,52,53]

Figure 8(a) illustrates the experimental setup for C-AFM measurements on the Al_2O_3 thin films on EG. In this configuration, current transport across the insulating layers is probed with nanoscale lateral resolution. A morphology map of the scanned area is reported in **Figure 8(b)**, which includes both uniform Al_2O_3 on 1L EG and Al_2O_3 on a 2L EG patch. **Figures 8(c)-(e)** show current maps collected on this area with increasing positive values of the tip bias with respect to EG, i.e. $V_{\text{tip}}=3$ V (c), 6 V(d) and 9 V(e). While uniform low current values are

detected in all the considered bias range through the 12 nm Al_2O_3 film onto 1L EG, the onset of high current spots is observed in the 2L EG region at a tip bias of 6V (see Figure 8(d)). These current leakage spots expand within the 2L EG region when V_{tip} is further increased to 9 V (Figure 8(e)).

Figure 8(f) illustrates two representative local current-voltage characteristics collected by the C-AFM probe on Al_2O_3 in the 1L and 2L EG regions. While current smoothly increases with the bias for Al_2O_3 on 1L EG, an abrupt rise of current is observed for $V_{\text{tip}} > 6\text{V}$ in the case of Al_2O_3 on 2L EG. This locally enhanced conduction in the 2L EG area can be justified by the less compact Al_2O_3 structure and the lower average thickness detected in these regions. By adopting a simplified planar capacitor model for the tip/ Al_2O_3 /EG system, a breakdown field $> 8\text{ MV/cm}$ can be estimated for the 12 nm Al_2O_3 on 1L EG. The high leakage current spots observed in the 2L EG regions indicate premature breakdown events, with a breakdown field of $\sim 6\text{ MV/cm}$ estimated for an average Al_2O_3 thickness of $\sim 10\text{ nm}$ in these regions.

Current mapping and local I-V characteristics measured by C-AFM have the advantage of providing spatially resolved information on the conduction properties of the deposited Al_2O_3 insulator on 1L and 2L EG regions. Of course, when fabricating macroscopic contacts with several μm^2 areas, the 2L regions, even with a very low areal density, will represent the weaker points for device reliability. This suggests that further efforts must be dedicated to improve the EG thickness homogeneity, up to 100% 1L coverage.

3 Conclusions

In conclusion, uniform and conformal Al_2O_3 films were obtained by seed-layer-free thermal ALD on highly homogeneous monolayer EG grown under optimized high temperature conditions on on-axis 4H-SiC(0001). The enhanced nucleation behavior on 1L graphene is not

related to the SiC substrate, but it is peculiar of the EG/SiC interface. Ab-initio DFT calculations showed an enhanced adsorption energy for water molecules on highly n-type doped monolayer graphene, indicating the high doping of EG induced by the underlying buffer layer as the origin of the excellent Al₂O₃ nucleation. Nanoscale resolution current mapping by C-AFM showed highly uniform insulating properties of the Al₂O₃ thin films, with a breakdown field >8 MV/cm on monolayer EG. These results are expected to have important implications in epitaxial graphene device technology.

4 Experimental section

Materials preparation. The Al₂O₃ films were deposited by a thermal ALD process, using a PE-ALD LL SENTECH Instruments GmbH reactor. Trimethylaluminum (TMA) and water (H₂O) were used as aluminum and oxygen precursors, respectively. Both were delivered to the reactor chamber by nitrogen (N₂), as carrier gas, with a flow rate of 80 sccm. During the ALD cycle, pulse periods of 20 ms, for TMA and H₂O, were used coupled with a purging pulse of N₂ for 2 s, to remove unreacted precursors and to clean the deposition chamber. According to the nominal growth rate of 0.8 Å/cycle, a number cycles of 190 was used in order to deposit a Al₂O₃ thickness of ~15 nm. All depositions were carried out at the deposition temperature of 250°C and the pressure value of 10 Pa.

The ALD depositions of Al₂O₃ were carried out both on epitaxial graphene (EG) and transferred graphene (TG) on SiC. EG was grown both on “nominally” on-axis and 4° off- axis 4H-SiC (0001) by thermal decomposition at high temperature (2000 °C) in Ar ambient at atmospheric pressure using an inductively heated reactor. Thickness uniformity of the as-grown EG was evaluated by reflectance mapping using setup consisting of a modified micro-Raman spectrometer, as illustrated in Ref. ^[37]. The number of layers was calculated by comparison of reflectance values measured on bare 4H-SiC with those on SiC coated with 0L, 1L and 2L graphene.

Single layer graphene grown by chemical vapor deposition (CVD) on copper was also transferred to 4H-SiC (0001), with the transfer process consisting of the following steps: PMMA coating as support layer, chemical etching of copper with a solution of ammonium persulfate (APS), and graphene transfer printing to the SiC surface. Before graphene transfer, the native SiO₂ present on SiC surface was removed by a dip in HF. Furthermore, careful cleaning of the graphene surface by acetone and isopropanol was carried out after the transfer, in order to remove PMMA residuals.

Atomic force microscopy (AFM) measurements were carried out employing a D3100 microscope with Nanoscope V controller. Tapping mode morphology and phase images were acquired using Si tips with 5 nm curvature radius. Local current-voltage measurements and nanoscale current map were acquired by conductive atomic force microscopy (CAFM) using Pt-coated Si tips with 10 nm curvature radius.

Raman spectroscopy analyses were carried out using a Bruker SENTERRA spectrometer equipped with a confocal microscopy system and a 532 nm (2.33 eV) excitation laser at power lower than 5 mW. The best spectral resolution was equal to 9 cm⁻¹ and a data pitch equal to 0.5 cm⁻¹ was employed. After the acquisition, to evaluate the graphene Raman bands shift, the spectra were aligned to the Silicon band, which is located at 520.7 cm⁻¹.

High-resolution transmission electron microscopy (HR-TEM) analyses were carried out on FIB prepared cross-sectional samples to evaluate the thickness, structural and interfacial properties of Al₂O₃ layer on epitaxial graphene/SiC, using an FEI THEMIS 200 aberration corrected microscope transmission electron microscope.

DFT calculations. The Density Functional Theory was used for the evaluation of the adsorption energies of water molecules on charge-neutral and electron-doped graphene. Calculations were performed with the plane-wave Quantum Espresso code,^[54] using the Perdew-Burke-Ernzerhof exchange-correlation functional^[55] along with ultrasoft pseudopotentials.^[56] The studied systems comprised of periodic (5×5) graphene supercells interacting with a single H₂O

molecule each, and separated by 15 Å from their replicas along the direction perpendicular to the graphene plane. Electronic convergence was obtained with a plane-wave cutoff kinetic energy of 35 Ry and an augmented charge density cutoff of 280 Ry. The Brillouin zone was sampled with a Monkhorst-Pack k -point grid^[57] of $4\times 4\times 1$, while for the definition of the Fermi level, single-point calculations with a grid of $24\times 24\times 1$ were performed on the relaxed structures. The adsorption energy was defined as $E_{ads} = E_{gr+H_2O} - (E_{gr} + E_{H_2O})$, where E_{gr+H_2O} and E_{gr} were the total energies of the graphene/H₂O and bare graphene system, respectively, under the same charge conditions, whereas E_{H_2O} was the reference energy for a single H₂O molecule. In order to properly evaluate the binding between H₂O and graphene, van der Waals corrections were considered in the computational model within the DFT-D scheme,^[58,59] giving rise to adsorption energy estimates with a very good agreement when compared to higher order methods.^[60] In order to simulate the doping conditions of EG on SiC(0001), we performed calculations by gradually increasing the charge of the system by steps of $-0.1e$, until reaching the experimental charge value of epitaxial graphene ($\sim 1.5\times 10^{13}$ cm⁻² achieved at a charge value of $-0.3e$ for our supercell model).

A similar approach has been used to evaluate the adsorption energy of the TMA molecule on graphene surface as a function of the Fermi level position of graphene.

Supporting Information

Supporting Information is available from the Wiley Online Library.

Acknowledgements

The authors want to acknowledge A. Kakanakova (Linköping University), P. Fiorenza (CNR-IMM, Catania), I. Cora and L. Toth (HAS-MTA, Budapest) for useful discussions. S. Di Franco (CNR-IMM, Catania) is acknowledged for technical support in sample preparation. This work has been funded, in part, by the FlagERA projects GraNitE (MIUR grant no. 0001411) and

GRIFONE. Part of the experimental activities have been carried out in the framework of the CNR-HAS Bilateral project GHOST. B.P. thanks the financial support of OTKA 118914 project (Hungary). R.Y. thanks the RMA- and GMT- SSF programs (Sweden) for financial support.

Received: ((will be filled in by the editorial staff))

Revised: ((will be filled in by the editorial staff))

Published online: ((will be filled in by the editorial staff))

References

-
- ¹ Y.-M. Lin, C. Dimitrakopoulos, K. A. Jenkins, D. B. Farmer, H.-Y. Chiu, A. Grill, Ph. Avouris, 100-GHz Transistors from Wafer-Scale Epitaxial Graphene, *Science* **2010**, 327, 662.
 - ² A. A. Sagade, D. Neumaier, D. Schall, M. Otto, A. Pesquera, A. Centeno, A. Z. Elorza, H. Kurz, Highly Air Stable Passivation of Graphene Based Field Effect Devices. *Nanoscale* **2015**, 7, 3558–64.
 - ³ T.-E. Bae, H. Kim, J. Jung, W.-J. Cho, Fabrication of High-Performance Graphene Field-Effect Transistor with Solution-Processed Al₂O₃ Sensing Membrane. *Appl. Phys. Lett.* **2014**, 104, 153506.
 - ⁴ F. Giannazzo, G. Greco, F. Roccaforte and S. S. Sonde, Vertical Transistors Based on 2D Materials: Status and Prospects, *Crystals* **2018**, 8, 70.
 - ⁵ W. Mehr, J. Dabrowski, J. C. Scheytt, G. Lippert, Y. H. Xie, M. C. Lemme, M. Östling, G. Lupina, Vertical Graphene Base Transistor. *IEEE Electron Device Lett.* **2012**, 33, 691–693.
 - ⁶ F. Giannazzo, G. Fisichella, G. Greco, A. La Magna, F. Roccaforte, B. Pecz, R. Yakimova, R. Dagher, A. Michon, Y. Cordier, Graphene Integration with Nitride Semiconductors for High Power and High Frequency Electronics. *Phys. Status Solidi A* 2016, 1–16.
 - ⁷ A. Pakkala, M. Putkonen, in *Handb. Depos. Technol. Film. Coatings, Elsevier*, **2010**, pp. 364–391.
 - ⁸ R. H. J. Vervuurt, W. M. M. Kessels, A. A. Bol, Atomic Layer Deposition for Graphene Device Integration, *Adv. Mater. Interfaces* **2017**, 4, 1700232.

- ⁹ B. Lee, S. Park, H.-C. Kim, K. Cho, E. M. Vogel, M. J. Kim, R. M. Wallace, J. Kim, Conformal Al₂O₃ dielectric layer deposited by atomic layer deposition for graphene-based nanoelectronics, *Appl. Phys. Lett.* **2008**, 92, 203102.
- ¹⁰ Z. R. Robinson, G. G. Jernigan, V. D. Wheeler, S. C. Hernández, C. R. Eddy, T. R. Mowll, E. W. Ong, C. A. Ventrice, H. Geisler, I. Pletikosic, H. Yang, T. Valla, Growth and characterization of Al₂O₃ films on fluorine functionalized epitaxial graphene, *J. Appl. Phys.* **2016**, 120, 075302
- ¹¹ N. Y. Garces, V. D. Wheeler, J. K. Hite, G. G. Jernigan, J. L. Tedesco, Neeraj Nepal, C. R. Eddy Jr., D. K. Gaskill, Epitaxial graphene surface preparation for atomic layer deposition of Al₂O₃, *J. Appl. Phys.* **2011**, 109, 124304
- ¹² V. K. Sangwan, D. Jariwala, S. A. Filippone, H. J. Karmel, J. E. Johns, J. M. P. Alaboson, T. J. Marks, L. J. Lauhon, M. C. Hersam, Quantitatively Enhanced Reliability and Uniformity of High- κ Dielectrics on Graphene Enabled by Self-Assembled Seeding Layers, *Nano Lett.* **2013**, 13, 1162.
- ¹³ S. Kim, J. Nah, I. Jo, D. Shahrjerdi, L. Colombo, Z. Yao, E. Tutuc, S. K. Banerjee, Realization of a High Mobility Dual-Gated Graphene Field-Effect Transistor with Al₂O₃ Dielectric. *Appl. Phys. Lett.* **2009**, 94, 062107.
- ¹⁴ B. Fallahazad, K. Lee, G. Lian, S. Kim, C. M. Corbet, D. A. Ferrer, L. Colombo, E. Tutuc, Scaling of Al₂O₃ Dielectric for Graphene Field-Effect Transistors. *Appl. Phys. Lett.* **2012**, 100, 093112.
- ¹⁵ M. J. Hollander, M. LaBella, Z. R. Hughes, M. Zhu, K. A. Trumbull, R. Cavalero, D. W. Snyder, X. Wang, E. Hwang, S. Datta, J. A. Robinson, Enhanced Transport and Transistor Performance with Oxide Seeded High-k Gate Dielectrics on Wafer-Scale Epitaxial Graphene, *Nano Lett.* **2011**, 11, 3601–3607.
- ¹⁶ Y. Zhang, Z. Qiu, X. Cheng, H. Xie, H. Wang, X. Xie, Y. Yu, R. Liu, Direct Growth of High-Quality Al₂O₃ Dielectric on Graphene Layers by Low-Temperature H₂O-Based ALD. *J. Phys. D: Appl. Phys.* **2014**, 47, 055106.
- ¹⁷ L. Zheng, X. Cheng, D. Cao, G. Wang, Z. Wang, D. Xu, C. Xia, L. Shen, Y. Yu, D. Shen, Improvement of Al₂O₃ Films on Graphene Grown by Atomic Layer Deposition with Pre-H₂O Treatment. *ACS Appl. Mater. Interfaces* **2014**, 6, 7014–7019.
- ¹⁸ G. Fisichella, E. Schilirò, S. Di Franco, P. Fiorenza, R. Lo Nigro, F. Roccaforte, S. Ravesi, F. Giannazzo, Interface Electrical Properties of Al₂O₃ Thin Films on Graphene Obtained by Atomic Layer Deposition with an in Situ Seedlike Layer, *ACS Applied Materials & Interfaces* **2017**, 9, 7761-7771.

- ¹⁹ X. Wang, S. M. Tabakman, H. Dai, Atomic Layer Deposition of Metal Oxides on Pristine and Functionalized Graphene. *J. Am. Chem. Soc.* **2008**, *130*, 8152.
- ²⁰ B. Karasulu, R. H. J. Vervuurt, W. M. M. Kessels, A. A. Bol, Continuous and ultrathin platinum films on graphene using atomic layer deposition: a combined computational and experimental study. *Nanoscale* **2016**, *8*, 19829.
- ²¹ K. Kim, H.-B.-R. Lee, R. W. Johnson, J. T. Tanskanen, N. Liu, M.-G. Kim, C. Pang, C. Ahn, S. F. Bent, Z. Bao, Selective metal deposition at graphene line defects by atomic layer deposition. *Nat. Commun.* **2014**, *5*, 4781.
- ²² A. I. Aria, K. Nakanishi, L. Xiao, P. Braeuninger-Weimer, A. A. Sagade, J. A. Alexander-Webber, S. Hofmann, Parameter Space of Atomic Layer Deposition of Ultrathin Oxides on Graphene, *ACS Appl. Mater. Interfaces* **2016**, *8*, 30564–30575.
- ²³ R. H. J. Vervuurt, B. Karasulu, M. A. Verheijen, W. (Erwin) M. M. Kessels, A. A. Bol, Uniform atomic layer deposition of Al₂O₃ on graphene by reversible hydrogen plasma functionalization. *Chem. Mater.* **2017**, *29*, 2090.
- ²⁴ Y. Zhang, Q. Fu, Y. Cui, R. Mu, L. Jin, X. Bao, Enhanced reactivity of graphene wrinkles and their function as nanosized gas inlets for reactions under graphene. *Phys. Chem. Chem. Phys.* **2013**, *15*, 19042.
- ²⁵ Q. Wu, Y. Wu, Y. Hao, J. Geng, M. Charlton, S. Chen, Y. Ren, H. Ji, H. Li, D. W. Boukhvalov, R. D. Piner, C. W. Bielawski, R. S. Ruoff, Selective surface functionalization at regions of high local curvature in graphene. *Chem. Commun.* **2013**, *49*, 677.
- ²⁶ B. Dlubak, P. R. Kidambi, R. S. Weatherup, S. Hofmann, J. Robertson, Substrate-assisted nucleation of ultra-thin dielectric layers on graphene by atomic layer deposition. *Appl. Phys. Lett.* **2012**, *100*, 173113.
- ²⁷ C. Berger, Z. Song, X. Li, X. Wu, N. Brown, C. Naud, D. Mayou, T. Li, J. Hass, A. N. Marchenkov, E. H. Conrad, P. N. First, W. A. de Heer, Electronic confinement and coherence in patterned epitaxial graphene. *Science* **2006**, *312*, 1191-1196.
- ²⁸ C. Virojanadara, M. Syvajarvi, R. Yakimova, L. I. Johansson, A. A. Zakharov, and T. Balasubramanian, Homogeneous large-area graphene layer growth on 6H-SiC(0001). *Phys. Rev. B* **2008**, *78*, 245403.
- ²⁹ K. V. Emtsev, A. Bostwick, K. Horn, J. Jobst, G. L. Kellogg, L. Ley, J. L. McChesney, T. Ohta, S. A. Reshanov, J. Röhrl, E. Rotenberg, A. K. Schmid, D. Waldmann, H. B. Weber, T. Seyller. Towards wafer-size graphene layers by atmospheric pressure graphitization of silicon carbide. *Nature Materials* **2009**, *8*, 203-207.

- ³⁰ A. Tzalenchuk, S. Lara-Avila, A. Kalaboukhov, S. Paolillo, M. Syvajarvi, R. Yakimova, O. Kazakova, T.J.B.M.Janssen, V. Fal'ko, and S. Kubatkin, Towards a quantum resistance standard based on epitaxial graphene, *Nature Nanotechnology* **2010**, 5, 186-189.
- ³¹ C. Melios, V. Panchal, K. Edmonds, A. Lartsev, R. Yakimova, O. Kazakova, Detection of Ultralow Concentration NO₂ in Complex Environment Using Epitaxial Graphene Sensors, *ACS Sens.* **2018**, 3, 1666–1674.
- ³² F. Varchon, R. Feng, J. Hass, X. Li, B. Ngoc Nguyen, C. Naud, P. Mallet, J.-Y. Veullen, C. Berger, E. H. Conrad, L. Magaud, Electronic Structure of Epitaxial Graphene Layers on SiC: Effect of the Substrate, *Phys. Rev. Lett.* **2007**, 99, 126805.
- ³³ I. Deretzis, A. La Magna, Role of covalent and metallic intercalation on the electronic properties of epitaxial graphene on SiC (0001), *Phys. Rev. B* **2011**, 84, 235426.
- ³⁴ C. Riedl, A. A. Zakharov, U. Starke, C. Riedl, Precise in situ thickness analysis of epitaxial graphene layers on SiC(0001) using low-energy electron diffraction and angle resolved ultraviolet photoelectron spectroscopy, *Appl. Phys. Lett.* **2008**, 93, 033106.
- ³⁵ F. Speck, M. Ostler, J. Rohrl, K. V. Emtsev, M. Hundhausen, L. Ley, Th. Seyller, Atomic layer deposited aluminum oxide films on graphite and graphene studied by XPS and AFM, *Phys. Status Solidi C* **2010**, 7, 398–401.
- ³⁶ J. A. Robinson, M. LaBella, K. A. Trumbull, X. Weng, R. Cavelero, T. Daniels, Z. Hughes, M. Hollander, M. Fanton, D. Snyder, Epitaxial Graphene Materials Integration: Effects of Dielectric Overlayers on Structural and Electronic Properties, *ACS Nano* **2010**, 4, 2667–2672.
- ³⁷ I. G. Ivanov, J. Ul Hassan, T. Iakimov, A. A. Zakharov, R. Yakimova, E. Janzén, Layer-number determination in graphene on SiC by reflectance mapping, *Carbon* **2014**, 77, 492-500
- ³⁸ C. Vecchio, S. Sonde, C. Bongiorno, M. Rambach, R. Yakimova, V. Raineri, and F. Giannazzo, Nanoscale structural characterization of epitaxial graphene grown on off-axis 4H-SiC (0001). *Nanoscale Res. Lett.* **2011**, 6, 269.
- ³⁹ G. Nicotra, I. Deretzis, M. Scuderi, C. Spinella, P. Longo, R. Yakimova, F. Giannazzo, A. La Magna. Interface disorder probed at the atomic scale for graphene grown on the C face of SiC, *Phys. Rev. B* **2015**, 91, 15541.
- ⁴⁰ J. Haeberle, K. Henkel, H. Gargouri, F. Naumann, B. Gruska, M. Arens, M. Tallarida, D. Schmeißer, Ellipsometry and XPS comparative studies of thermal and plasma enhanced atomic layer deposited Al₂O₃-films, *Beilstein J. Nanotechnol.* **2013**, 4, 732-742.
- ⁴¹ S. C. Ha, E. Choi, S.- H. Kim, J. S. Roh, Influence of oxidant source on the property of atomic layer deposited Al₂O₃ on hydrogen-terminated Si substrate, *Thin Solid Films* **2005**, 476 , 252.

- ⁴² R. Nakamura, M. Ishimaru, H. Yasuda, H. Nakajima. Atomic rearrangements in amorphous Al_2O_3 under electron-beam irradiation, *Journal of Applied Physics* **2013**, 113, 064312.
- ⁴³ D. Su Lee, C. Riedl, B. Krauss, K. von Klitzing, U. Starke, J. H. Smet, Raman Spectra of Epitaxial Graphene on SiC and of Epitaxial Graphene Transferred to SiO_2 , *Nano Lett.* **2008**, 8, 4320-4325.
- ⁴⁴ G. Fisichella, S. Di Franco, F. Roccaforte, S. Ravesi, F. Giannazzo. Microscopic mechanisms of graphene electrolytic delamination from metal substrates. *Appl. Phys. Lett.* **2014**, 104, 233105.
- ⁴⁵ A. Das, S. Pisana, B. Chakraborty, S. Piscanec, S. K. Saha, U. V. Waghmare, K. S. Novoselov, H. R. Krishnamurthy, A. K. Geim, A. C. Ferrari, A. K. Sood, Monitoring dopants by Raman scattering in an electrochemically top-gated graphene transistor, *Nat. Nanotechnol.* **2008**, 3, 210-215.
- ⁴⁶ J. E. Lee, G. Ahn, J. Shim, Y.S. Lee, S. Ryu, Optical separation of mechanical strain from charge doping in graphene, *Nat. Commun.* **2012**, 3, 1024.
- ⁴⁷ F. Fromm, M. H. Oliveira Jr., A. Molina-Sanchez, M. Hundhausen, J. M. J. Lopes, H. Riechert, L. Wirtz, T. Seyller, Contribution of the buffer layer to the Raman spectrum of epitaxial graphene on SiC(0001), *New Journal of Physics* **2013**, 15, 043031.
- ⁴⁸ M. A. Bissett, S. Konabe, S. Okada, M. Tsuji, H. Ago, Enhanced Chemical Reactivity of Graphene Induced by Mechanical Strain, *ACS Nano* **2013**, 7, 10335–10343.
- ⁴⁹ M. J. Park, H.-H. Choi, B. Park, J. Y. Lee, C.-H. Lee, Y. S. Choi, Y. Kim, J. M. Yoo, H. Lee, B. H. Hong, Enhanced Chemical Reactivity of Graphene by Fermi Level Modulation, *Chem. Mater.* **2018**, 30, 5602–5609.
- ⁵⁰ G. Hong, Y. Han, T. M. Schutzius, Y. Wang, Y. Pan, M. Hu, J. Jie, C. S. Sharma, U. Muller, D. Poulidakos, On the Mechanism of Hydrophilicity of Graphene, *Nano Lett.* **2016**, 16, 7, 4447-4453.
- ⁵¹ C. E. Giusca, V. Panchal, M. Munz, V. D. Wheeler, L. O. Nyakiti, R. L. Myers-Ward, D. K. Gaskill, O. Kazakova, Water Affinity to Epitaxial Graphene: The Impact of Layer Thickness, *Adv. Mater. Interfaces* **2015**, 2, 1500252.
- ⁵² S. Sonde, F. Giannazzo, V. Raineri, R. Yakimova, J.-R. Huntzinger, A. Tiberj, and J. Camassel, Electrical properties of the graphene/4H-SiC (0001) interface probed by scanning current spectroscopy, *Phys. Rev. B* **2009**, 80, 241406(R).
- ⁵³ F. Giannazzo, G. Fisichella, G. Greco, P. Fiorenza, F. Roccaforte, in *Conductive Atomic Force Microscopy: Applications in Nanomaterials* (Ed: M. Lanza), WILEY-VCH Verlag, Weinheim 2017, Ch. 7, pp. 163– 186. ISBN: 978-3-527-34091-0.

-
- ⁵⁴ P. Giannozzi, S. Baroni, N. Bonini, M. Calandra, R. Car, C. Cavazzoni, D. Ceresoli, L. C. Guido, M. Cococcioni, I. Dabo, A. Dal Corso, S. de Gironcoli, S. Fabris, G. Fratesi, R. Gebauer, U. Gerstmann, C. Gougoussis, A. Kokalj, M. Lazzeri, L. Martin-Samos, N. Marzari, F. Mauri, R. Mazzarello, S. Paolini, A. Pasquarello, L. Paulatto, C. Sbraccia, S. Scandolo, G. Sclauzero, A.P. Seitsonen, A. Smogunov, P. Umari and R.M. Wentzcovitch, QUANTUM ESPRESSO: a modular and open-source software project for quantum simulations of materials. *J. Phys.: Condens. Matter* **2009**, *21*, 395502.
- ⁵⁵ J. P. Perdew, K. Burke, M. Ernzerhof, *Phys. Rev. Lett.* **1996**, *77*, 3865–3868.
- ⁵⁶ D. Vanderbilt, *Phys. Rev. B* **1990**, *41*, 7892.
- ⁵⁷ H. J. Monkhorst and J. D. Pack, *Phys. Rev. B* **1976**, *13*, 5188–5192.
- ⁵⁸ S. Grimme, *Journal of computational chemistry*, **2006**, *27*, 1787-1799.
- ⁵⁹ V. Barone, M. Casarin, D. Forrer, M. Pavone, M.Sambi, and A. Vittadini, *Journal of computational chemistry*, **2009**, *30*, 934-939.
- ⁶⁰ I. Hamada, *Phys. Rev. B* **2012**, *86*, 195436.

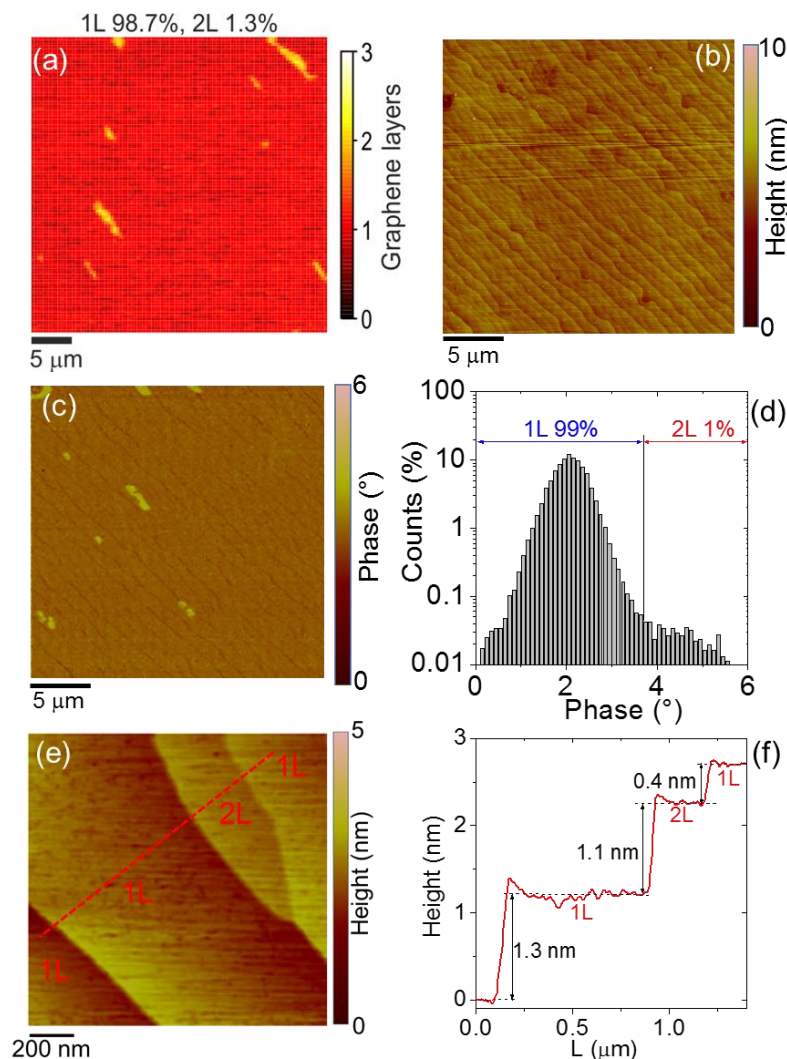


Figure 1 (a) Reflectance map of as-grown EG collected on a $30\ \mu\text{m} \times 30\ \mu\text{m}$ sample area. The red contrast background is associated to 1L graphene (98.7% of total area) and the yellow elongated patches to 2L graphene (1.3% of total area). (b) AFM morphology and (c) phase map on a $30\ \mu\text{m} \times 30\ \mu\text{m}$ sample area. The small elongated patches with higher phase contrast correspond to 2L Gr. (d) Histogram of phase values extracted from the phase map: the main peak at lower phases is associated to 1L graphene covered regions and a small shoulder at higher phases the 2L graphene patches. 1L coverage of 99% and 2L coverage of 1% evaluated by integration of the counts under the two peaks. (e) Higher resolution AFM morphology and (f) height line-scan of 1L EG including a 2L patch.

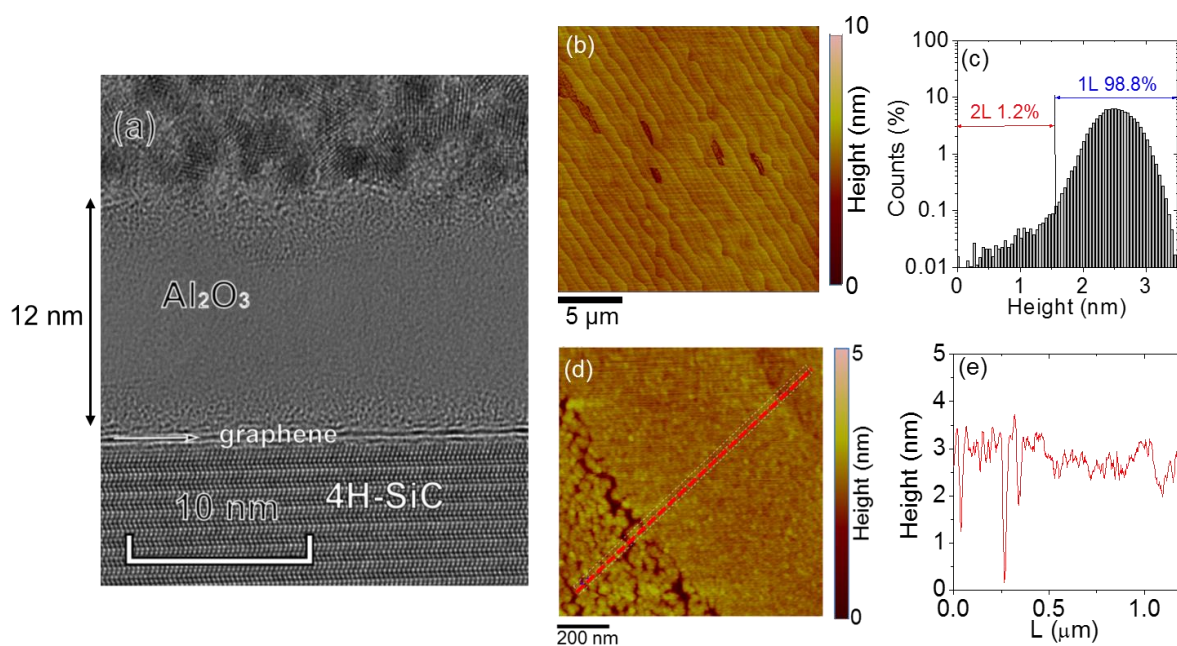


Figure 2 (a) Cross-sectional TEM image of the Al₂O₃ film deposited on 1L EG on SiC. (b) AFM morphology on 20 μm × 20 μm scan area and (c) corresponding histogram of height values, showing uniform and conformal Al₂O₃ coverage on 1L graphene and small depressions on 2L graphene. Higher resolution AFM morphology (d) and height linescan (e) of Al₂O₃ at the boundary region between 1L EG and a 2L patch. A compact Al₂O₃ film with small grains is observed on top of 1L EG, whereas Al₂O₃ with larger grains separated by small depressions (up to 2 nm) is observed on the 2L EG region.

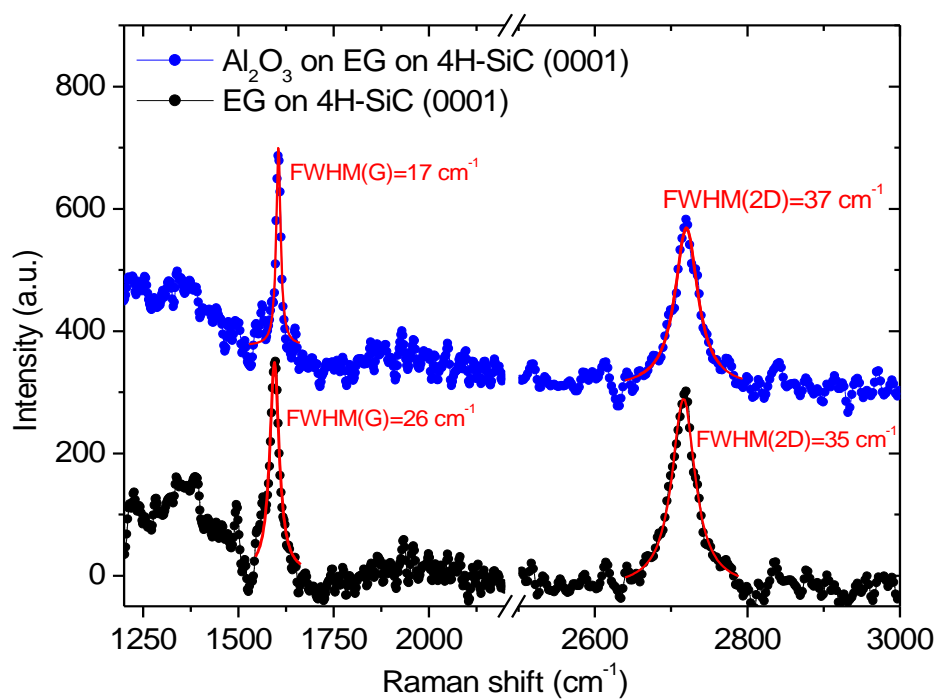


Figure 3. Representative Raman spectra of virgin EG and after the Al_2O_3 deposition

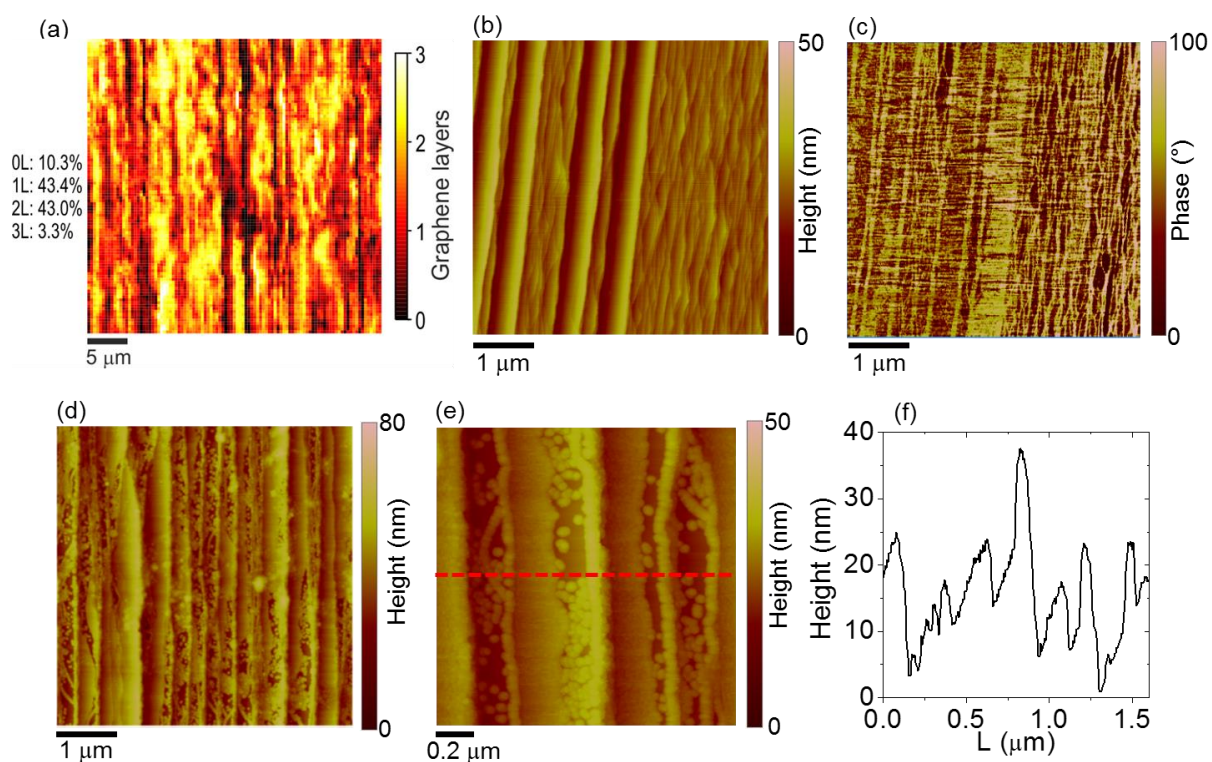


Figure 4. (a) Reflectance (b) AFM morphology and (c) phase map of EG grown by thermal decomposition of a 4°-off SiC(0001) substrate. The evaluated percent coverage of 0L (~10.3%), 1L (~43.4%), 2L (~43%) and 3L (~3.3%) are reported in (a). AFM morphologies at different magnifications ((d) and (e)) of the Al₂O₃ deposited on this EG sample, showing the coexistence of regions covered by a continuous Al₂O₃ film with partially or totally uncovered regions. (f) Height linescan extracted along the line indicated in (e).

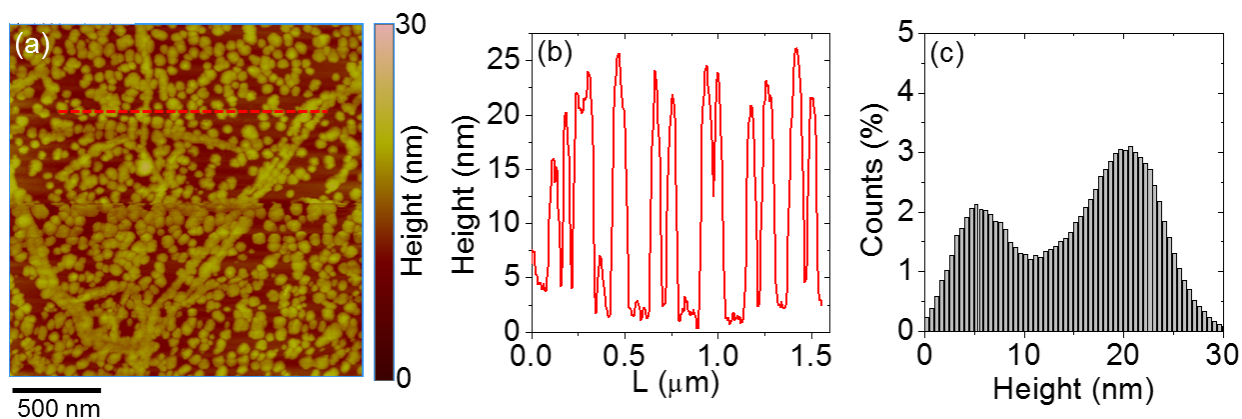


Figure 5. (a) AFM morphology and representative (b) height linescan of Al₂O₃ deposited by ALD onto TG on SiC. (c) Histogram of the height values extracted from (a), showing a bimodal distribution with two very distinct peaks, corresponding to the uncovered and Al₂O₃-covered graphene areas.

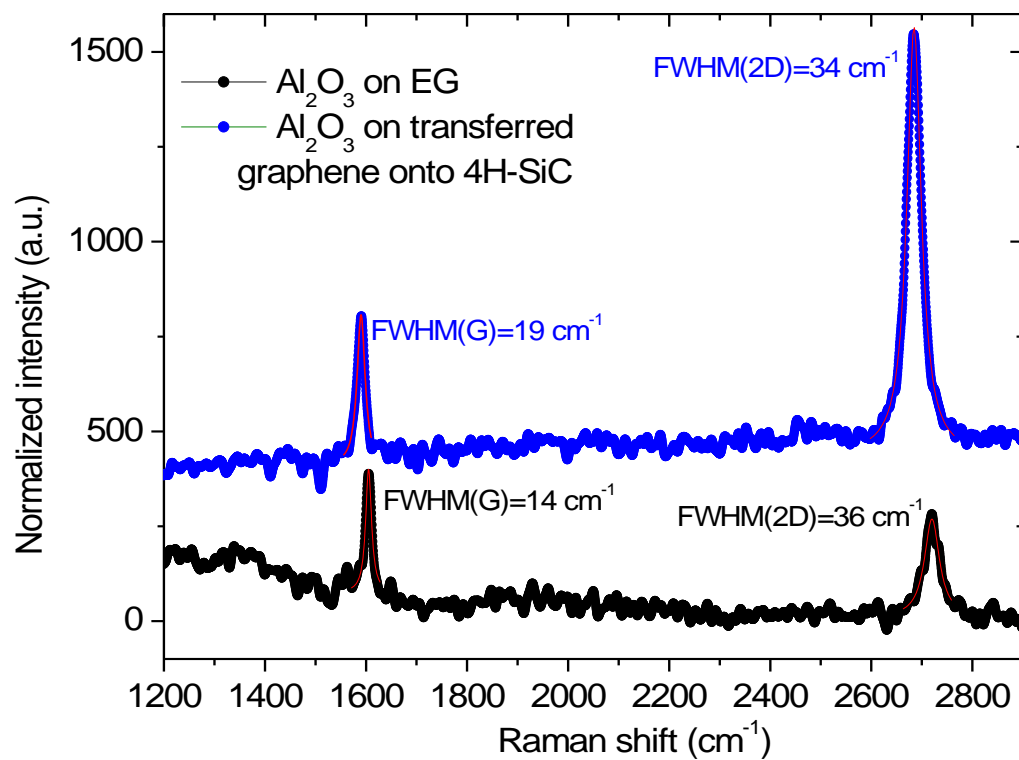


Figure 6. Raman spectra of monolayer EG and of TG onto 4H-SiC(0001), after ALD of 15 nm Al₂O₃.

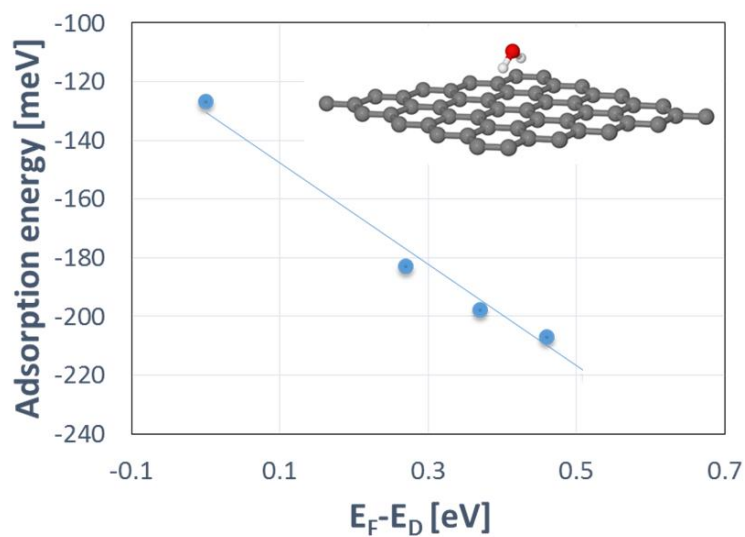


Figure 7. DFT calculation of the adsorption energy of a water molecule on monolayer graphene by changing the Fermi level position with respect to the Dirac point ($E_F - E_D$), from 0 (neutral graphene) to 0.45 eV, corresponding to n-type doping of $\sim 1.5 \times 10^{13} \text{ cm}^{-2}$.

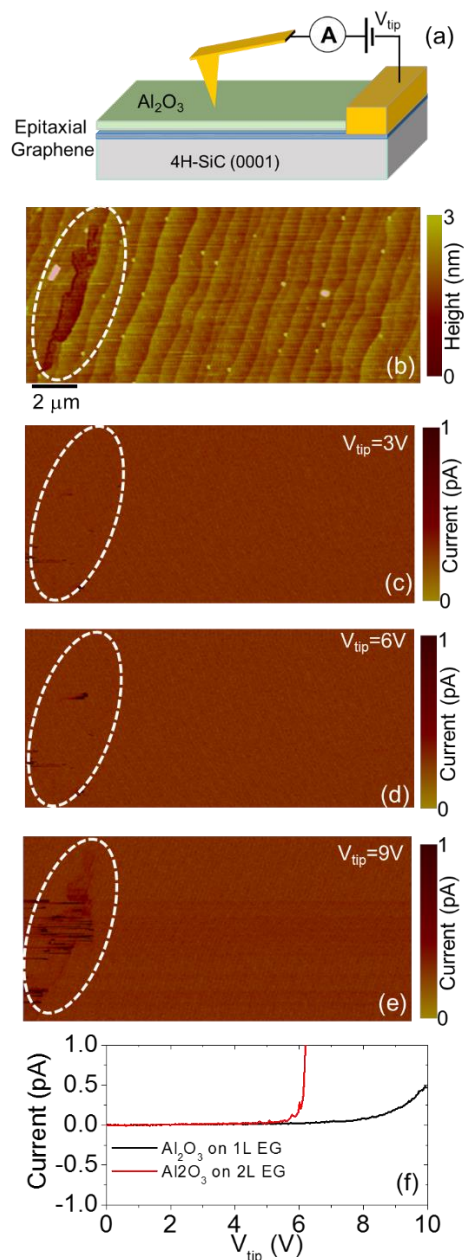


Figure 8 (a) Schematic representation of the C-AFM setup for local current mapping through the Al₂O₃ thin film deposited onto EG on axis 4H-SiC(0001). (b) Morphology of the probed sample area, including both uniform Al₂O₃ on 1L EG and Al₂O₃ on a 2L EG patch. (c)-(e) Current maps collected on this area with increasing tip bias with respect to EG, i.e. V_{tip}=3 V (c), 6 V(d) and 9 V(e). (f) Two representative local current-voltage characteristics collected by the C-AFM probe on Al₂O₃ in the 1L and 2L EG regions.